6

Medical Image Registration with Fourier basis Functions

Roberto A. Isoardi[1], Amílcar R. Osorio[2] and Germán Mato[3]
[1]*Fundación Escuela de Medicina Nuclear, Mendoza*
[2]*Fundación Centro Diagnóstico Nuclear, Buenos Aires*
[3]*Grupo Física Estadística, Centro Atómico Bariloche, Bariloche*
Argentina

1. Introduction

Registration is one of the most interesting, yet challenging computer-aided tasks in medical image processing, aimed at bringing two or more data sets into spatial and/or temporal correlation. If the represented data are medical images, there are countless situations where it is of interest to attain such correlation, as it has become routine practice in many diagnostic and image-guided therapeutic procedures.

For example, one of the most frequent clinical applications is to align two scans of a given patient, e.g. for easy identification of equivalent structures on both registered images, follow-up of disease, etc. Another use of image registration is commonplace during brain activation studies, where several functional Magnetic Resonance (*f*MRI) or Positron Emission Tomography (PET) scans are repeated on the same or different subjects while receiving sensorial or cognitive stimulations. In order to perform a statistical analysis on the brain images, it is often necessary to register all data sets with respect to a brain atlas. In this way, both statistical power and signal-to-noise ratio are enhanced in what is known as intra-modality registration (Friston et al, 2006).

One of the most exciting applications is inter-modality registration, e.g. correlating PET and MR (Magnetic Resonance) scans of a same subject, or PET vs. CT (Computed Tomography). PET imaging provides distinctive functional and metabolic information, but lacks the high anatomical resolution which is in turn provided by conventional MR or CT. Thus PET/CT registration is synergic, since it facilitates the location of malignancies in their anatomical context. Moreover, this modality combination is often useful for Radiotherapy Planning (Townsend, 2008).

An automatic image registration algorithm normally includes a *floating image* to be aligned to the coordinate system of a *reference image*. To do this, a spatial transformation function –containing a number of parameters-, must be proposed and applied to the former data set. The parameters are chosen in such a way that a proposed *similarity measure* between both data sets is optimized. This measure may be –for example-, the Normalized Mutual Information (NMI) or the Cross Correlation Coefficient.

Methods which apply rigid-body transformations perform reasonably well for registering images of the head (brain) and extremity portions. In a 3D space, a rigid-body transformation involves only six parameters, e.g. three translations (Δx, Δy, Δz) and three

rotation angles (θ_x, θ_y, θ_z). A natural extension of the rigid approach is the use of *affine* transformations that include scaling and shearing (Maintz & Viergever, 1998).

However, those simple transformations often yield unacceptable results when dealing with deformable body regions such as thorax and abdomen. Even with a careful repositioning on the scanner table, the body region of interest may displace between different scans with respect to the scanner coordinate system, due to various reasons, which may include voluntary and involuntary motion (e.g. respiration, cardiac function), misplacement errors, variations in morphology and physiology, etc.

Several non-rigid or deformable methods have been widely explored to treat this problem (Crum et al, 2004)(Rueckert & Aljabar, 2010). This is an open field of research, both for its complexity and situations of interest. Unlike rigid models, deformable registration is particularly difficult to validate with clinical images, where internal fiducial markers are not available. Besides, the optimization of the objective function may be non-unique or even physically meaningless.

Nevertheless, the main complexity of a deformable system lies on its many degrees of freedom. In an extreme situation, it would be necessary to propose a 3D independent transformation for each image voxel. In this case, the number of transformations would be three times the number of voxels. To treat this problem a set of approximations is implemented, otherwise the optimization would be very costly in such a parameter space. Most methods apply a rigid transformation as a first approximation, and then improve registration with a non-rigid approach with a small set of *basis functions*.

These functions form the basis for a vector space, where any function can be represented as a linear combination of those basis functions. They can be polynomial $\{1, t, t^2\}$, just like those used to build splines (Bookstein 1989). For instance, spline basis functions are used when fiducial markers are available or with physical model-based algorithms (e.g. elastic deformations, viscous fluids, etc) (D'Agostino et al, 2003).

One particular kind of functions that make up an orthonormal basis are trigonometric $\{sin(n\pi x), cos(n\pi x)\}$, where $n \geq 0$ is the order of the basis function. In this chapter we present a systematic analysis for the deformable registration problem using trigonometric Fourier basis functions (Ashburner & Friston, 1999). With these functions, the typical size of the deformation field can be easily controlled, ranging from long to short wavelengths. By combining this approach with a volume subdivision scheme, we expect to apply a small set of basis functions at a given stage of the algorithm. In principle, given that Fourier functions make a complete set, any arbitrary deformation may be approximated only by increasing the number of basis functions.

In our study, we analyze intra-modality registration (CT-CT, MR-MR, PET-PET) in 3D. For each modality, we determine the optimum number of coefficients (transformation order) for the basis functions and the number of subvolumes to attain a satisfactory registration within a reasonable computing time.

As a similarity measure, we calculate the Normalized Mutual Information (NMI) for different transformation orders and applying the algorithm in the thoraco-abdominal region. Each clinical volume data set was artificially deformed using a known displacement field, in order to simulate an inhalation expansion, and then co-registered to its original counterpart, taken as the reference image. In order to evaluate its clinical usefulness, we also apply this method to co-register two scans of the same subject, each one acquired on different dates. In a previous work, we established and tried this methodology in 2D (Osorio

et al, 2007). In this chapter, we extend it to 3D, including parameter optimization analysis (Osorio et al, 2010).

2. The image registration process

The aim of a registration procedure is to attain spatial alignment of one or more images – which we shall call "floating" (B), with respect to another one taken as the "reference" image (A). In a very general framework, given image A with coordinates $\mathbf{r_A}$, and image B with coordinates $\mathbf{r_B}$, we search the transformation:

$$\mathbf{T} : \mathbf{r}_B \rightarrow \mathbf{r}_A$$

such that: $$\mathbf{T}(\mathbf{r}_B) = \mathbf{r}_A \text{ and } max_T[S(A,B)]$$

where S(A,B) is a *similarity measure* between A and B, usually represented by an objective function. For most cases, the similarity measure is critical for the success and general performance of the registration process. Its choice depends on the use of extrinsic or intrinsic image properties (e.g. fiducial markers or pixel intensity values), body region, modalities, matrix dimensions, etc. If the registration algorithm is iterative, another essential component is the *optimizer* for function S, which necessarily involves multiple evaluations in a multidimensional parameter space (Hill & Batchelor, 2001). The process is complete when a termination criterion is met.

Transformation $\mathbf{T}$ describes a spatial mapping from $\mathbf{r}_B$ to $\mathbf{r}_A$. In terms of elasticity, transformations may be rigid, affine, projective or curve (van den Elsen et al, 1993). The simplest transformation is the rigid one, requiring only 6 parameters in 3D (3 translations + 3 rotation angles). An affine transformation keeps parallelism between lines, introducing scaling and shearing (12 parameters in 3D). After a general projective transformation, line straightness is conserved, though parallelism is lost. Finally, a curved transformation produces a deformation that may be arbitrarily complex, though some constraints may apply to preserve smoothness and topology (e.g. each voxel should keep the same neighbours after applying the deforming transformation). As introduced in the previous section, the rigid model provides satisfactory results when the body region is limited to the head and some limb portions. To account for non-rigid displacements that may happen in the body, we adopt the scheme described in the next section.

3. Fourier-based registration: theoretical grounds

We have devised the following algorithm for non-rigid registration of image volumes A and B, each consisting of a stack of tomographic slices:

1. Pre-processing: segmentation, resampling, filtering.
2. An initial registration is carried out by applying an affine transformation (rigid+scaling), B ->A, optimizing the Normalized Mutual Information as a similarity measure (to be described later on).
3. B is divided into k sub-volumes B_r (k=8 in 3D).
4. An independent transformation is applied to each portion B_r , with a rigid and a non-rigid component.
5. The global transformation $T_{global}=S\ (T_1 \cup T_2 ... \cup T_k\ )$ is obtained after assembling the transformations T_r .

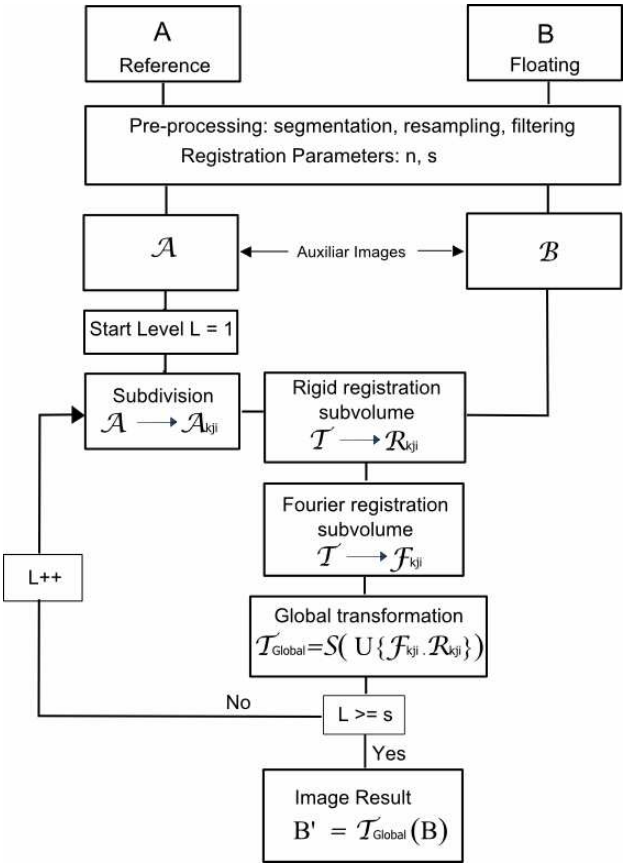

Fig. 1. Flowchart of the whole registration algorithm

Fig. 1 shows a diagram of this algorithm. After the initial affine approach in steps 2 and 4, the non-rigid stage is performed by a *n*-order Fourier expansion along each dimension:

$$T_x(\mathbf{r}) = x + \sum_{i,j,k=1}^{n} \left[a_{ijk}\varphi_{ijk}(\mathbf{r}) + b_{ijk}\psi_{ijk}(\mathbf{r}) \right] \tag{1}$$

$$T_y(\mathbf{r}) = y + \sum_{i,j,k=1}^{n} \left[c_{ijk}\varphi_{ijk}(\mathbf{r}) + d_{ijk}\psi_{ijk}(\mathbf{r}) \right] \tag{2}$$

$$T_z(\mathbf{r}) = z + \sum_{i,j,k=1}^{n} \left[e_{ijk}\varphi_{ijk}(\mathbf{r}) + f_{ijk}\psi_{ijk}(\mathbf{r}) \right] \tag{3}$$

where:

$$\varphi_{ijk}(\mathbf{r}) = \sin\left(\frac{\pi i x}{X}\right)\sin\left(\frac{\pi j y}{Y}\right)\sin\left(\frac{\pi k z}{Z}\right),$$

and:

$$\psi_{ijk}(\mathbf{r}) = \cos\left(\frac{\pi i x}{X}\right)\cos\left(\frac{\pi j y}{Y}\right)\cos\left(\frac{\pi k z}{Z}\right).$$

X,Y,Z are the image dimensions and *a, b, c, d, e, f* the coefficients to find up to order *n*. The initial condition is randomly chosen with a Gaussian distribution $N(0,\sigma^2)$.
With this approach, functions φ_{ijk} represent the transformation subset that keeps the volume boundary invariant, whereas functions ψ_{ijk} represent the transformations with null gradient on that boundary.

4. Subdivision scheme

Once the rigid transformations are applied, the independent subvolumes were assembled using quaternion interpolation (Walimbe et al, 2004). Since there is no standard interpolation method adopted for non-rigid transformations, in this work we propose the strategy shown on Fig. 2. It consists of a hierarchical scheme where each volume is divided into 8 equal subvolumes, this process being repeated *s* times. In what follows, we shall refer to the variable *s* as the subdivision number. In this way we build up a global transformation which is smooth, continuous and differentiable. A detailed description of this strategy is developed in the Appendix of Osorio et al (2010).

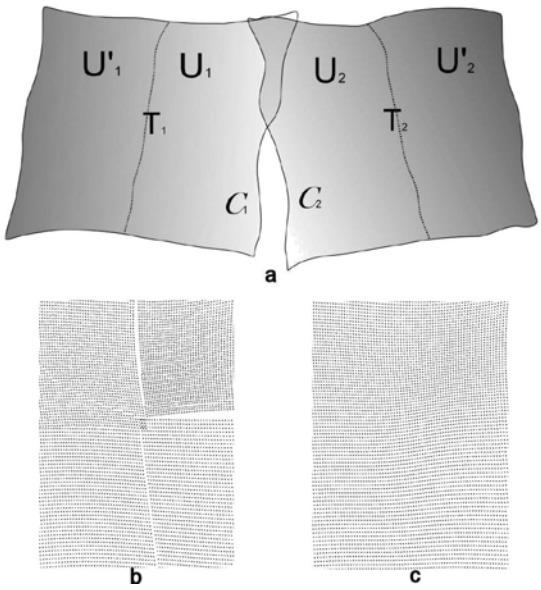

Fig. 2. a) Sub-volume assembling method. b) subvolumes before and c) after assembling. Figures show a 2D section of the 3D volume

5. Similarity measure and optimization

The metric adopted for this project is the Normalized Mutual Information, widely explored in the literature (Pluim et al, 2003), (Maes et al, 1997), (Studholme et al, 1999):

$$NMI = \frac{\sum_i p_i \log(p_i) + \sum_j p_j \log(p_j)}{\sum_{ij} p_{ij} \log(p_{ij})} \tag{4}$$

where p_i , p_j are the marginal probability distributions and p_{ij} is the joint distribution, using the partial volume method as interpolator (Chen et al, 2003).
The extended Downhill Simplex method was chosen as optimizer of the objective function (Press et al, 1992), (Zagrodsky et al, 2001). The program terminates when the change in the NMI is less than 10^{-4} between consecutive iterations.

6. Image data

Three tomographic modalities were studied: CT, MR and FDG[1]-PET of thorax and abdomen. For each one of those, we carried out a systematic analysis of the performance of intra-modality registration. CT studies were acquired with a HiSpeed scanner (GE, Milwaukee, USA) (matrix size: 512x512x47, voxel size: 0.7x0.7x7 mm^3). MRI studies were performed with a Signa Advantage 0.5 scanner (GE, Milwaukee, USA) (matrix size: 256x256x24) (voxel size 1.7x1.7x9 mm^3). The PET scanner used was a Quest 250 (UGM, Philadelphia, USA) (matrix size: 128x128x50, voxel size: 2x2x4 mm^3). All studies were completed at the Fundación Escuela de Medicina Nuclear (Mendoza, Argentina).
With the purpose of evaluating algorithm registration performance in a systematic way and for different initial conditions, we devised the following strategy. Each selected data set was slightly deformed using TPS (Thin-Plate Splines) (Bookstein, 1989)(Rohr et al, 2001) with a regular grid of 432 control points and average displacement of 27 mm (max. 40 mm), simulating a moderate thorax expansion during inhalation. This artificially deformed volume was selected as the floating image to be registered to the reference image (original, non-deformed version). This procedure was repeated for each modality, in order to find the parameters which maximize the NMI in a reasonable computing time.
Once the optimal Fourier order and subdivision number were found, we applied the algorithm to co-register pairs of thoraco-abdominal studies of a selected subject, which were acquired on different dates. In this way we had two data sets corresponding to the same body region, but displaying so evident anatomical discrepancies that would justify the application of a non-rigid model.

7. Error estimation

The error measure was chosen as the absolute average displacement over the whole image volume:

$$\varepsilon = \frac{1}{N} \sum_{i=1}^{N} \left| T(u_i) - \mathrm{v}_i \right| \tag{5}$$

where u_i and v_i are the voxel coordinates for the floating and reference images, respectively, and N is the total number of voxels.

[1] FDG: ^{18}F-labelled FluoroDeoxiGlucose

8. Registration of TPS-deformed image pairs

Fig. 3 shows the results corresponding to CT-CT registration after artificial deformation of the floating image. Shown are overlays of initial rigid registration and Fourier registration for transaxial slices. Coronal and sagittal overlays are shown in Fig. 4, which provide a visual assessment of our non-rigid approach. Bone structures remain unaltered during the process, which is consistent with a real situation.

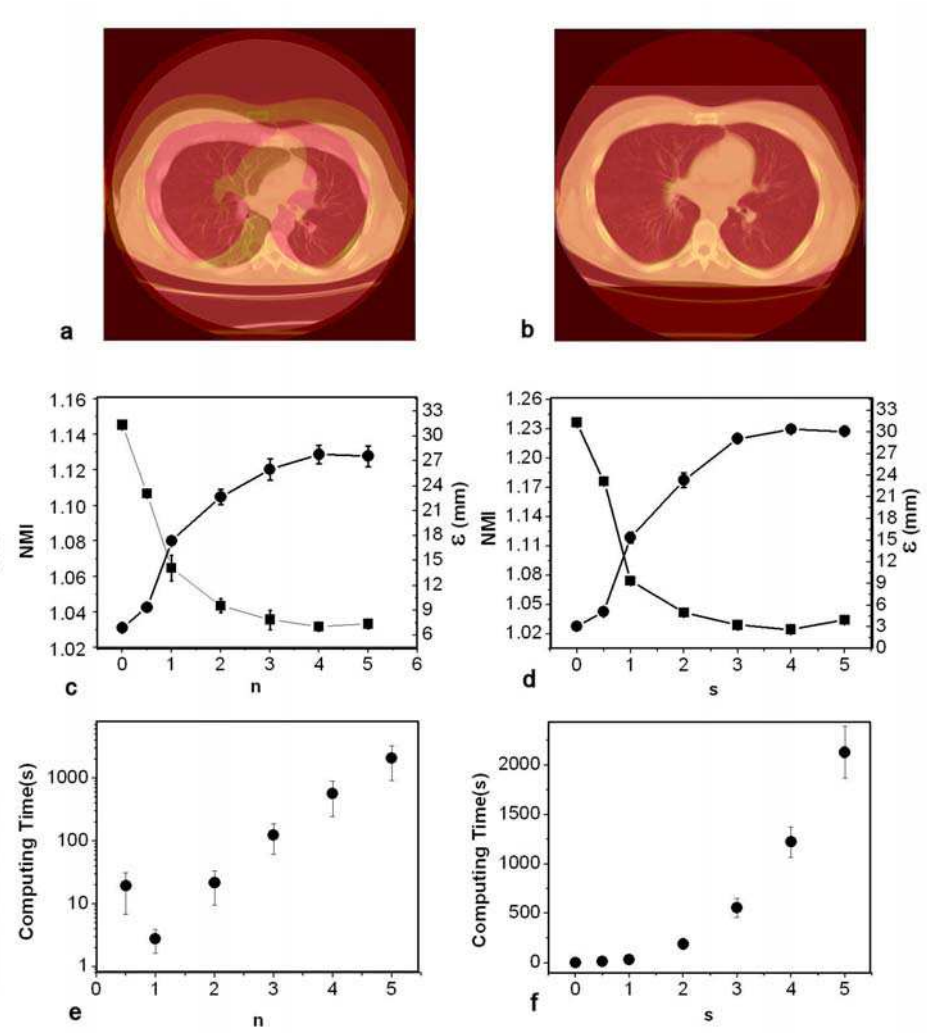

Fig. 3. CT vs. CT deformed with TPS (a) Rigid registration. (b) Fourier registration, n=2, s=4 (c) NMI (circles) and error ε (squares) vs. Fourier order for s=1. (d) NMI and error ε vs. number of subdivisions for n=2. (e) Computing time for Fig. 3c. (f) Computing time for Fig. 3d

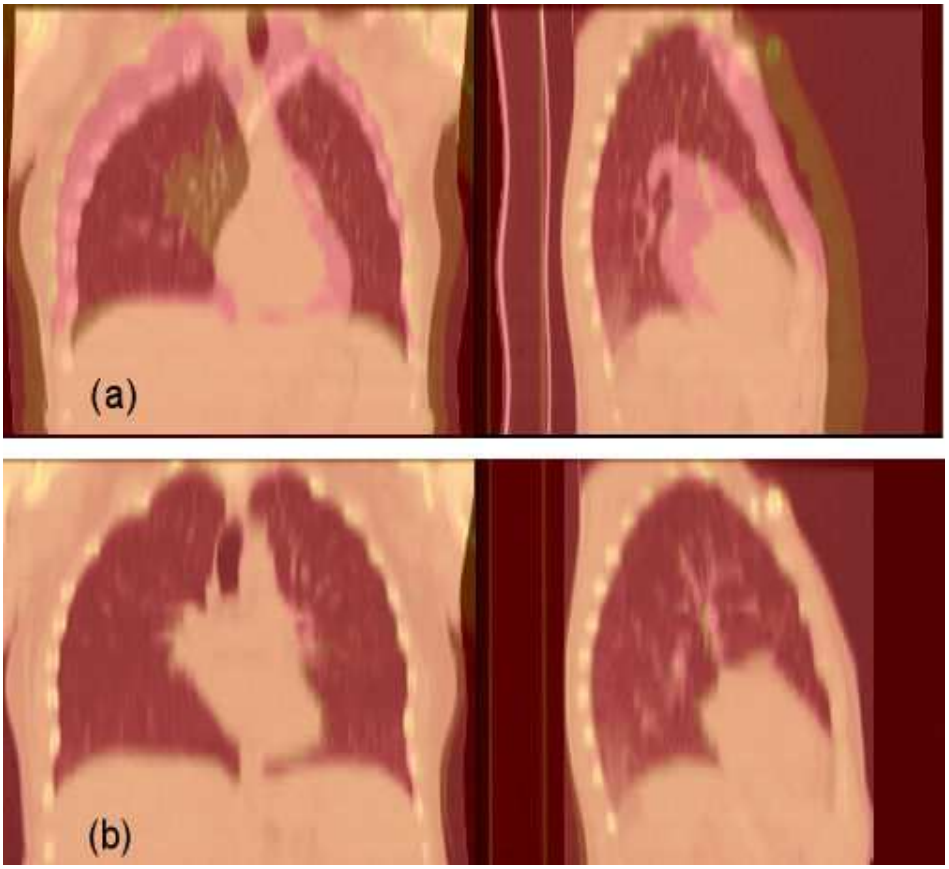

Fig. 4. Coronal and sagittal views of CT vs. TPS-deformed CT before (a) and after (b) Fourier registration

The graphs in Fig. 3 show the NMI, ε and computing time as a function of both the transformation order n and the subdivision number s. For all graphs, n,s=0 and n,s=0.5 refer to initial centre-of-mass alignment and rigid registration, respectively. Let us keep in mind that non-rigid registration comes into play when $n \geq 1$. As expected, the NMI increases and ε decreases at higher n. Looking for further optimization in the parameter space in a reasonable computing time, we set n=2 and plotted NMI vs. s. In this way, maximum NMI was attained at (n=2, s=4) for CT-CT registration. Each registration cycle was run 12 times, starting with different deformations, and the graphs show average values with their corresponding error bars. The computing time shows an exponential increase for n>1.

From the above results, we chose n=2 as the most appropriate transformation order, since at higher n values, error ε hardly decreases at the expense of long execution times. For the same reason, a suitable subdivision number was chosen at s=3,4. These results were also confirmed by visual inspection of the registered data sets.

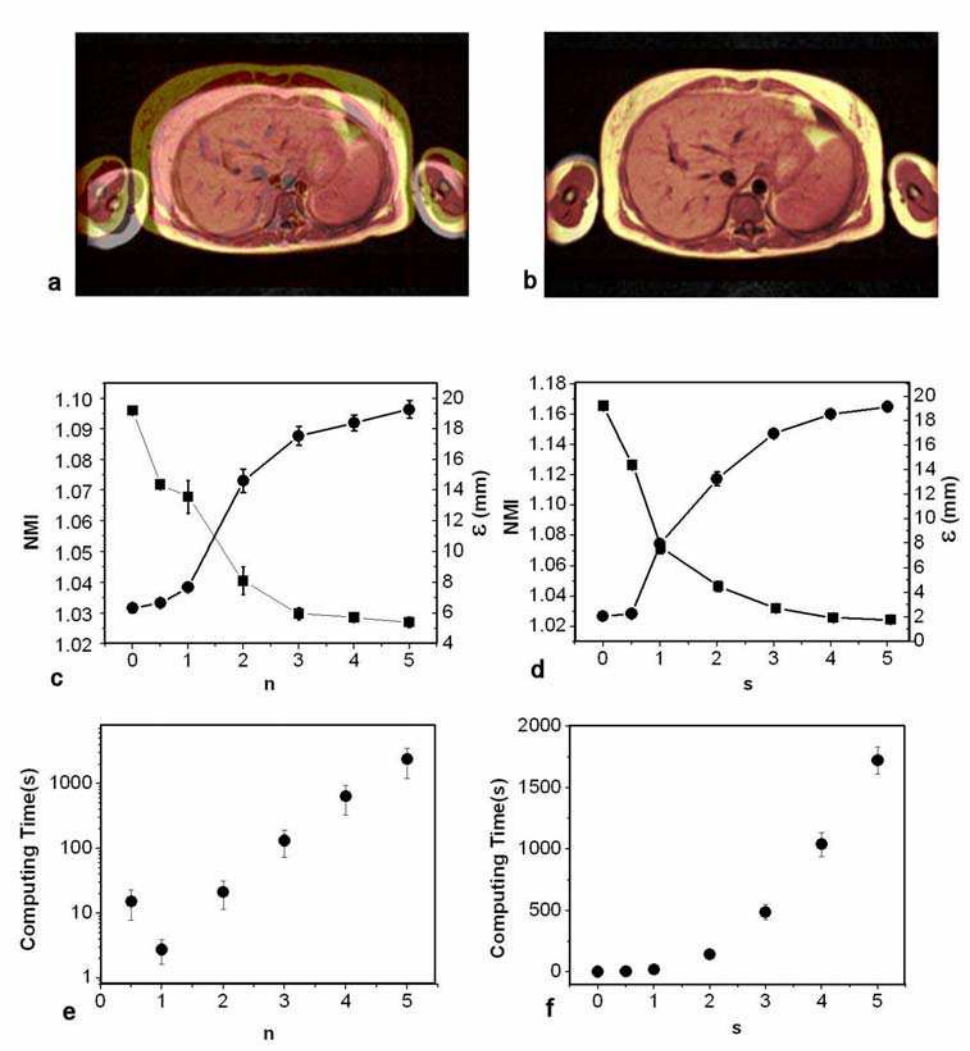

Fig. 5. MRI vs. MRI deformed with TPS (a) Rigid registration. (b) Fourier registration, n=2, s=4 (c) NMI (circles) and error ε (squares) vs. Fourier order for s=1. (d) NMI and error ε vs. number of subdivisions for n=2. (e) Computing time for Fig. 5c. (f) Computing time for Fig. 5d

Similar results were obtained for the MR-MR situation (Fig. 5). As for PET vs. PET, since it is a smaller dataset, no further improvement is obtained for s>3, when few voxels remain in each subvolume to calculate the NMI with enough statistical power.

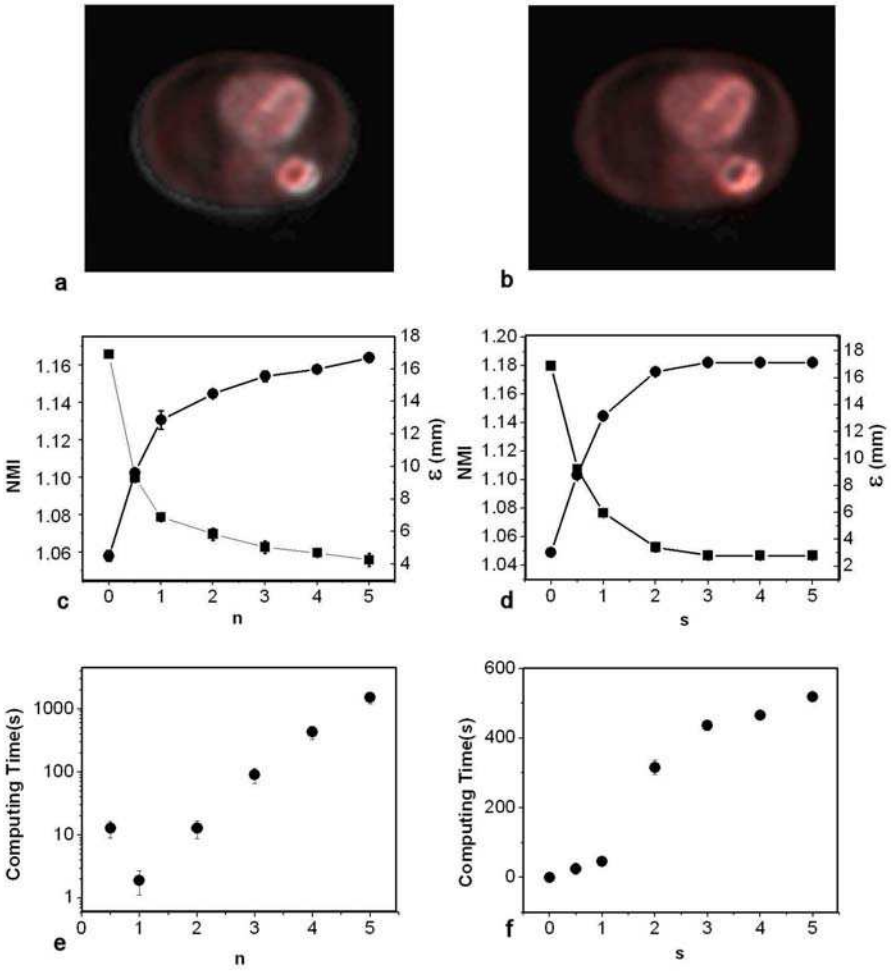

Fig. 6. PET vs. PET deformed with TPS (a) Rigid registration. (b) Fourier registration, n=2, s=4 (c) NMI (circles) and error ε (squares) vs. Fourier order for s=1. (d) NMI and error ε vs. number of subdivisions for n=2. (e) Computing time for Fig. 6c. (f) Computing time for Fig. 6d

9. Clinical studies

Once the optimum parameters were chosen from the previous analysis with TPS-deformed datasets, we selected three pairs of clinical studies to evaluate our method for intra-subject, intra-modality registration in real situations.

For each modality, the first study was taken as reference to which the second study was registered. Fig. 7 shows the results for all modalities, which were qualified by expert

radiologists as "acceptable" by visual inspection. The reader should keep in mind that in this case we lack from a "gold standard" for error calculation for obvious reasons, so this evaluation cannot be considered a validation test.

10. Error estimation with digital fiducial markers

Our choice for error estimation as described in Section 7, includes large portions of the field-of-view that are not relevant to registration process itself, such as the background that surrounds the body region of interest. To check if this has a significant impact on error calculation, 10 digital spheres were inserted in selected anatomical locations inside the CT, MR and PET volume data sets, so as to simulate easily identifiable internal fiducials. Next we applied a TPS deformation on such "marked" volumes and carry out the registration cycle as described in Section 8.

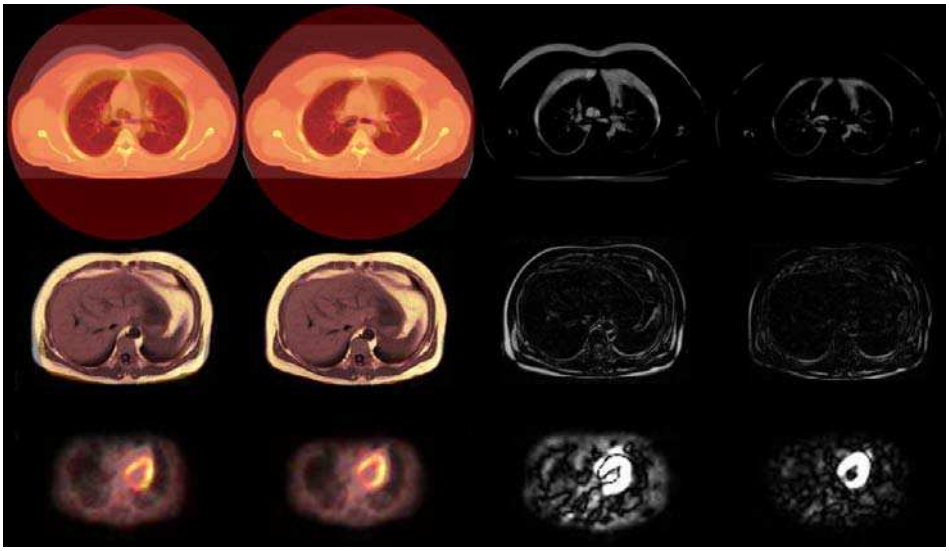

Fig. 7. Intra-modality registration of two clinical scans (same subject, different sessions). From left to right: Rigid registration, Fourier registration, Image difference after rigid registration, Image difference after Fourier registration. From top to bottom: CT, MRI and PET

After registration of both data sets, we measured the distance between center-of-masses for homologous spheres. Finally, the Mean Root Square Error (MRSE) was calculated using Eq. 5. In this case the summation is limited to the available sphere centers. In order to control for the effect of the additional deformation induced by the adjustments of the spheres on the registration, two different sphere sizes were studied: big (8 mm ϕ) and small (2 mm ϕ). The results are summarized in Table I, showing that the effect of the sphere size on the global error is quite small. This means that the spheres themselves are not affecting the registration process in a significative fashion.

We can see from Table 1 that the typical errors are between 1.5 mm and 2.5 mm, which are slightly smaller than the average displacements calculated for the whole volumes, as shown

in Figs. 3d, 5d and 6d. These results are of the same order as the ones found in recent approaches (Andronache et al, 2008), (Sohn et al, 2008) , using more complex methods such as a combination of cross-correlation and mutual information in the former and local matching of anatomical features in the latter. The computing time (as seen in Figs, 3, 5 and 6) is between 400 secs and 1000 secs, which is also of the same order as the time reported in the former reference.

	2 mm ϕ Sphere	8 mm ϕ Sphere	Error whole image
MRSE (CT)	2.55 mm	2.44 mm	2.62 mm
MRSE (MRI)	1.29 mm	1.55 mm	2.99 mm
MRSE (PET)	1.98 mm	1.58 mm	2.80 mm

Table 1. Mean Root Square Error (MRSE) for the three modalities (CT, MRI, PET). The errors in the second and third columns are evaluated after the registration with images that includes a set of 6 to 10 spheres. Sphere diameters are 2 mm and 8 mm. The error in the last column was evaluated over the whole image. The parameters of the algorithm were n=2, s=4 for CT and n=2, s=3 for MRI and PET

11. Discussion and conclusions

Our systematic analysis shows how the similarity measure (NMI) behaves with both the order of the transformation n and the number of subdivisions s. For intra-modality registration, and for the three modalities studied, we found that maximum NMI is attained for $n \geq 3$ (s=1). For n=2 the NMI is only slightly inferior, however the computing time becomes an order of magnitude longer if calculation is performed up to n = 3 (Figs. 3e, 4e, 5e), as the number of Fourier parameters to be optimized is $6n^3$ in 3D (Eqs. 1-3).

As expected, the similarity measure increases with the number of subdivisions s, accompanied by a decrease in error ε (Figs. 3d-5d). The improvement in registration quality was also confirmed by visual assessment for both CT-CT and MRI-MRI by comparing results using s=3 versus s=4. For PET-PET, NMI and ε does not get better for s>3, because further subdivision results in sub-volumes with too sparse data for that modality. Only slight improvements in the NMI and ε were recorded for n>3 and s>3, but at a very high computational cost and providing negligible visual improvements. One issue of concern is that rigid structures such as bone in CT should remain so after registration. Since the characteristic size of the deformation applied is greater than typical bone structures, they do not deform noticeably (Fig. 4).

Regarding calculation time, by setting optimal parameters (n=2, s=3), and using an ordinary computer[2], the time for co-registering two CT volumes (matrix dimensions 512×512×47) is ~ 600 secs. (~ 200 secs. if s=2). For MRI-MRI, somewhat shorter times were measured, whereas for PET-PET, execution took slightly over 400 secs. (Figs. 3f,5f,6f). Such computation times were attained without any specific optimization technique. Let us note that the algorithm leads naturally to parallelization because the subvolumes can be processed independently. In that way, the computing time can be substantially reduced.

In principle, the use of Fourier basis functions allows arbitrary deformations on any given image volume; the combination of this method with a subdivision scheme allows to

[2] Core 2 Duo, 3GHz, no multithreading (2008).

accommodate small image portions in a progressive fashion, without affecting the rest of the image data (Walimbe et al, 2004), (Likar & Pernus, 2001). Obviously, as the subdivision creates small subvolumes with fewer and fewer pixels, similarity measures like the NMI or the CCC become affected in their performance (Andronache et al, 2008).

In general, the proposed registration method rendered acceptable results for small and moderate deformations (~ 25mm). A preliminary study suggests that it is fairly robust, even in the presence of Gaussian noise (Osorio et al, 2007). We evaluated its performance using clinical images after deformation with Thin-Plate Splines, as well as image pairs corresponding to different scan sessions for a same subject. The selected studies were thoracic and abdominal scans for three common tomographic modalities. Obviously, not only organ deformations and displacements may come about between scan sessions, but also significant variations in anatomy and function, due to normal or pathological conditions. In these cases, the outcome of any non-rigid registration method offers an approximation whose usefulness must be assessed for each particular situation.

12. References

Andronache A.; von Siebenthal M.; Székely G. & Cattin P. (2008). Non-rigid registration of multi-modal images using both mutual information and cross-correlation. *Med. Imag. Anal.* 12, pp. 3-15.

Ashburner J. & Friston K. (1999). Nonlinear spatial normalization using basis functions. *Hum Brain Mapp*. Vol. 7, June 1999, pp. 254–266.

Bookstein F. (1989). Principal warps: Thin-plate splines and decomposition of deformations. *IEEE transactions on Pattern Analysis and Machine Intelligence,* 11:567-585.

Chen M. & Varshney P. K. (2003). Mutual information-based CT-MR brain image registration using generalized partial volume joint histogram estimation. *IEEE Trans. Med. Imaging* 22, pp. 1111-1119.

Crum W.; Hartkens T. & Hill D. (2004). Non-rigid image registration: theory and practice. *Br J Radiol*. Vol. 77: S140–S153.

D'Agostino E.; Maes F.; Vandermeulen D. & Suetens P. (2003). A viscous fluid model for multimodal non-rigid registration using mutual information. *Med Image Anal*. Vol. 7, December 2003, pp. 565-575.

Friston K.; Ashburner J.; Kiebel S.; Nichols T. & Penny W. (2006). *Statistical Parametric Mapping: The Analysis of Functional Brain Images*. ISBN-10: 0123725607 Academic Press, London.

Hill D. & Batchelor P. (2001). Registration Methodology: Concepts and Algorithms. En: Medical Image Registration (eds: Hajnal J.V. et al), CRC Press.

Likar B. & Pernus F. (2001). A Hierarchical Approach to Elastic Registration Based on Mutual Information. *Image Vis. Comput.* 19, pp. 33-44.

Maes F.; Collignon A.; Vandermeulen D.; Marchal G. & Suetens P. (1997). Multimodality image registration by maximization of mutual information. IEEE *Trans. Med. Imaging* 16, pp. 187-198.

Maintz J. & Viergever M. (1998). A survey of medical image registration. *Med Image Anal*. Vol. 2, March 1998, pp. 1–36.

Osorio A.; Isoardi, R. & Mato G. (2007). Non-rigid registration of tomographic images using Fourier transforms. *Journal of Physics: Conference Series. Vol.* 90, Issue 1, 2007, 012058

Osorio A.; Isoardi, R. & Mato G. (2010). Deformable CT registration using Fourier basis functions in 3D. In: *XXIII Brazilian Symposium on Computer Graphics and Image Processing (SIBGRAPI '2010), Gramado, IEEE Computer Society Press* (in press, September 2010).

Pluim J. P. W.; Maintz J. B. A. & Viergever M. A. (2003). Mutual-Information-Based Registration of Medical Images: A Survey. *IEEE Trans. Med. Imaging* 22, pp. 986-1004 .

Press W. H.; Flannery B. P.; Teukolsky S. A. & Vetterling W. T. (1992). Numerical Recipes in C: The Art of Scientific Computing, 2nd ed. (Cambridge University Press, Cambridge).

Rohr K.; Stiehl H. S.; Buzug T. M.; Weese J. & Kuhn M. H. (2001). Landmark-Based Elastic Registration Using Approximating Thin-Plate Splines. *IEEE Trans. Med. Imaging* 20, pp. 526-534.

Rueckert D. & Aljabar P. (2010). Non-rigid registration of medical images: theory, methods and applications. *IEEE Signal Proc. Mag*. Vol. 27, July 2010, pp. 113-119.

Sohn M.; Birkner M.; Chi Y.; Wang J.; Yan D.; Berger B. & Alber M. (2008). Model-independent, multimodality deformable image registration by local matching of anatomical features and minimization of elastic energy. *Med. Phys.* 35, pp. 866-878.

Studholme C.; Hill D. L. G. & Hawkes D. J. (1999). An overlap invariant entropy measure of 3D medical image alignment. *Pattern Recognit.* 32, pp. 71-86.

Townsend D. (2008). Multimodality imaging of structure and function, *Phys. Med. Biol.*, Vol. 53, February 2008: R1-R39.

van den Elsen P.; Pol E-J. D. & Viergever M. (1993). Medical image matching-a review with classification. *IEEE Eng. Med. Biol. Mag*. Vol. 12, March 1993, pp. 26-39.

Walimbe V. S.; Zagrodsky V.; Raja S.; Bybel B.; Kanvinde M. & Shekhar R. (2004). Elastic registration of three-dimensional whole body CT and PET images by quaternion-based interpolation of multiple piecewise linear rigid-body registrations, *Proceedings of the SPIE* (SPIE, San Diego, CA, 2004), pp. 1191–1228.

Zagrodsky V.; Shekhar R. & Cornhill J. F. (2001). Multi-function extension of simplex optimisation method for mutual information based registration of ultrasound volumes. *Proc. SPIE* 4322, pp. 508-515.

Fourier Transforms - New Analytical Approaches and FTIR Strategies

Edited by Prof. Goran Nikolic

ISBN 978-953-307-232-6
Hard cover, 520 pages
Publisher InTech
Published online 01, April, 2011
Published in print edition April, 2011

New analytical strategies and techniques are necessary to meet requirements of modern technologies and new materials. In this sense, this book provides a thorough review of current analytical approaches, industrial practices, and strategies in Fourier transform application.

How to reference

In order to correctly reference this scholarly work, feel free to copy and paste the following:

Roberto A. Isoardi, Amîlcar R. Osorio and Germán Mato (2011). Medical Image Registration with Fourier basis Functions, Fourier Transforms - New Analytical Approaches and FTIR Strategies, Prof. Goran Nikolic (Ed.), ISBN: 978-953-307-232-6, InTech, Available from: http://www.intechopen.com/books/fourier-transforms-new-analytical-approaches-and-ftir-strategies/medical-image-registration-with-fourier-basis-functions

INTECH
open science | open minds

InTech Europe
University Campus STeP Ri
Slavka Krautzeka 83/A
51000 Rijeka, Croatia
Phone: +385 (51) 770 447
Fax: +385 (51) 686 166
www.intechopen.com

InTech China
Unit 405, Office Block, Hotel Equatorial Shanghai
No.65, Yan An Road (West), Shanghai, 200040, China
中国上海市延安西路65号上海国际贵都大饭店办公楼405单元
Phone: +86-21-62489820
Fax: +86-21-62489821